

Cobalt Hydroxide Nanoflakes Prepared by Saccharide-Assisted Cathodic Electrochemical Deposition as High Performance Supercapacitor Electrode Material

Mustafa Aghazadeh¹, Mohammad Reza Ganjali^{2,3,*} and Mohammad Ghannadi Maragheh¹

¹ Material and Nuclear Research School, Nuclear Science and Technology Research Institute (NSTRI), P.O. Box 14395-834, Tehran, Iran

² Center of Excellence in Electrochemistry, School of Chemistry, University of Tehran, Tehran, Iran

³ Biosensor Research Center, Endocrinology and Metabolism Molecular-Cellular Sciences Institute, Tehran University of Medical Sciences, Tehran, Iran

*E-mail: ganjali@khayam.ut.ac.ir

Received: 4 March 2017 / Accepted: 16 April 2017 / Published: 12 May 2017

Cobalt hydroxide flake-like nanostructures are prepared through green electrochemical synthesis procedure. In this way, an aqueous solution of 0.005M cobalt chloride and 1g/L starch was used as an electrosynthesis bath. The cobalt hydroxide deposit was prepared in a two-electrode system containing stain less steel cathode and graphite anode by applying current density of 10 mA cm⁻². The structural characterization by XRD, IR, FE-SEM and TEM confirmed that the deposited sample is composed of β -cobalt hydroxide with flake-like morphology. The charge storage ability of the prepared nanoflakes was further evaluated using cyclic voltammetry (CV), galvanostat charge-discharge (GCD) cycling and electrochemical impedance spectroscopy (EIS). The electrochemical measurement revealed that the prepared cobalt hydroxide has low equivalent series resistance (R_s) and charge transfer resistance (R_{ct}), which enabled the fabricated electrode to deliver specific capacitances as high as 1125.4, 992, 849.3, 701.6 and 452.5 F g⁻¹ at 1, 2, 3, 5 and 10 A g⁻¹, respectively, and capacity retentions 93.48% and 80.17% after 2000 GCD at the current loads of 1 and 5 A g⁻¹. These results supported the proper characteristics of the prepared nanomaterials for the supercapacitor applications.

Keywords: Cobalt hydroxide; Flake structures; Green Electrosynthesis; Supercapacitive performance

1. INTRODUCTION

As very promising green energy storage devices, offering considerable power density and cycling lives, supercapacitors have found different applications from back-up power supplies and mobile electronic devices to sources of hybrid vehicles. These devices are commonly built based on

electrodes made of macro and nano-structured metal oxides or graphene/metal oxides composite [1-8]. Instances of the nano structured metal salts used as the electroactive materials in building supercapacitor electrodes include nano-particles [9-11], nano-wires plates or sheets [12-20], nano-spheres [21-23], nano-belts [24], nano-rods[24-27], nano-capsules [28-30] and nano-worms [31]. The application of nano-materials has been due to the advantages offered thereby including the ease of their large-scale preparation, and fast redox kinetics which greatly improve the specific capacitances (SCs), cycle lives and power densities of the resulting supercapacitors.

From the different metal compounds cobalt oxide and hydroxide are rather interesting compounds due to their low price and abundance, as well as high theoretical charge storage capacities. The latter has a hexagonal layered structure and is found as polymorphic crystalline forms known as α and β [32]. The α cobalt hydroxide is isostructural hydrotalcite-like compound, while the β form has a brucite-like $[\text{Mg}(\text{OH})_2]$ structure, which consists of hexagonally packed OH^- ions with Co^{2+} present at alternate rows of the octahedral sites. When prepared through electrochemical procedures, these mostly form plates or sheets that have large interlayer spacing due to intercalated anions such as nitrate, chloride, sulfate, etc [32-34]. The large interlayer spacings in these materials allow for access increased access by the electrolyte species to the electroactive material due to the facilitated penetration of the electrolyte and rapid ion transfer [35]. In sheet or plate morphologies where the particles have low thickness and high porosity the materials offer interesting electrochemical performance, due to the high surface area of the material and the subsequently high number of charge storage sites, which shortens the diffusion paths of ions. The high number of pores, on the other hand, leads to improved penetration of the electrolyte. All in all, these greatly improve the specific capacities, cycle performances and fast chargeability of devices using cobalt hydroxide as the electrode material. In this regard, many researchers have reported various synthetic routes for preparation of nano-plates/sheets of cobalt hydroxide with enhanced charge storage performances [36-42]. For example, Cheng *et al.* prepared α - $\text{Co}(\text{OH})_2$ nanosheets exfoliated graphene layers through a facile scalable solution method, and the prepared hybrid material provided a high specific capacitance of 567.1 F g^{-1} at 1 A g^{-1} [36]. Nguyen *et al.* electrodeposited nickel-cobalt hydroxide nanosheets on carbon nanofoam paper, and observed the areal capacity/capacitance values of $1.52 \text{ C cm}^{-2}/2.03 \text{ F cm}^{-2}$ at the current load of 2.1 mA cm^{-2} [37]. Cobalt hydroxide nanoplates doped with Al^{3+} ions have been also prepared through hydrothermal method [38], and the specific capacity value of 709.1 F g^{-1} , and capacity retention of 95.8% have been calculated at a current density of 1 A g^{-1} . A three-dimensional (3D) sponge-like $\text{Co}/\text{Co}(\text{OH})_2$ nanocomposite has been synthesized by a simple NaBH_4 reduction method at room temperature, which delivered a good specific capacity of 1048 F g^{-1} at a current density of 1 A g^{-1} [39]. Meng *et al.* reported solvothermal synthesis of mixed cobalt/nickel hydroxides with specific capacitance of 855.4 C g^{-1} at 1 A g^{-1} [41]. $\text{Co}(\text{OH})_2$ nanocubes have been fabricated via reacting $\text{Co}_3[\text{Co}(\text{CN})_6]_2$ nanocubes with NaOH aqueous solution which exhibited 420 F g^{-1} at 1 A g^{-1} [42].

This work is based on the optimization of a green cathodic electrosynthesis method for preparing nanostructured cobalt hydroxide, in an aqueous solution of cobalt chloride (0.005M) + 1 g/L sucrose. The product was found to be flake-like β - $\text{Co}(\text{OH})_2$ as indicated by XRD, IR, SEM, and TEM analyses. The electrochemical evaluation of the charge storage ability of the resulting product was

through cyclic voltammetry (CV), galvanostatic charge-discharge (GCD) and electrochemical impedance spectroscopy (EIS) revealed these nanoflakes to show high pseudo-capacitor performances, as indicated by an SC of 1125.4 F g^{-1} at 1 A g^{-1} and a 93.4% capacity retention of after 2000 GCD cycles.

2. EXPERIMENTAL SECTION

2.1. Chemicals

$\text{Co}(\text{NO}_3)_2 \cdot 6\text{H}_2\text{O}$ (Merck), polytetrafluoroethylene (PTFE, Merck), sucrose ($\text{C}_{12}\text{H}_{22}\text{O}_{11}$, Sigma-Aldrich), acetylene black and KOH (Merck) were used as received. All solutions were prepared by using purified water prepared by a UHQ Elga System. An aqueous solution of $0.005 \text{ MCoCl}_2 \cdot 6\text{H}_2\text{O}$ was prepared and used as electro-deposition electrolyte.

2.2. Electrosynthesis of cobalt hydroxide

1.189g cobalt chloride ($\text{CoCl}_2 \cdot 6\text{H}_2\text{O}$) and 1 gr sucrose were dissolved in 1 liter aqueous water and used as the deposition bath. The electrochemical set up includes a stainless steel (316L, surface area 100 cm^2) cathode placed between two graphite anodes. The hydroxide deposit was obtained on direct current mode with applying current density of 10 mA cm^{-2} . The deposition time and bath temperature were 30 min and $40 \text{ }^\circ\text{C}$, respectively. After deposition, the steel cathode was washed several times with the deionized water and dried at $80 \text{ }^\circ\text{C}$ for 1h. The deposit was then scraped from the steel surface and the obtained green powder was collected and characterized by various analyses.

2.3. Characterization techniques

The surface morphology of prepared powder were observed by field-emission Scanning electron microscopy (FE-SEM, Mira 3-XMU with accelerating voltage of 100 kV) and transmission electron microscopy (TEM, Phillips EM 208 with an accelerating voltage of 100 kV). The crystal structure of the prepared sample was determined by X-ray diffraction of powder (XRD, Phillips PW-1800) using $\text{Cu K}\alpha$ radiation. FT-IR spectrum was provided through a Bruker Vector 22 FT-IR spectrometer within the wave numbers of $400\text{-}4000 \text{ cm}^{-1}$. Cyclic voltammetry (CV) and galvanostatic charge-discharge (GCD) profiles were recorded using a potentiostat (AUTOLAB[®], Eco Chemie, PGSTAT 30). A three-electrode set up including the working electrode (cobalt hydroxide paste), reference electrode (Ag/AgCl , 1 M KCl, saturated), the counter electrode (platinum wire), and 1M KOH aqueous electrolyte. The working paste was fabricated by mixing the prepared cobalt hydroxide, acetylene black, conducting graphite and polytetrafluoroethylene (PTFE) binder (with the weight ratios of 75:10:10:5, respectively). The prepared mixture was pressed under 10 MPa into steel mesh current collectors ($1 \text{ cm} \times 1 \text{ cm}$) and then dried in oven for 10 min at $70 \text{ }^\circ\text{C}$. The CVs of the working electrode were recorded in 1M KOH solution at the potential window of -0.2 and 0.5 V vs.

Ag/AgCl. The various the scan rates of 2, 5, 10, 25, 50 and 100 mV s^{-1} were applied in the CV tests. The specific capacitances of the working electrode were determined from the CV profiles using Eq. (1) [17]:

$$C = \frac{Q}{m \Delta V}, \quad Q = \int_{V_a}^{V_b} I(V) dV \quad (1)$$

where C is the capacitance of cobalt hydroxide (F g^{-1}), Q is total charge, ΔV is the applied potential window, m is the mass of cobalt hydroxide used in the fabricated electrode (g), v is the scan rate (V s^{-1}) and $I(V)$ is a current response during the scan of potential. The mass loading of active materials was 2.4 mg . The charge-discharge curves were obtained at the current loads of 1, 2, 3, 5 and 10 A g^{-1} within a potential range of -0.2 to 0.5 V vs. Ag/AgCl. The following formula was used for the calculating the specific capacitances of the prepared sample at the applied current loads:

$$C = \frac{Q}{m \times \Delta V}, \quad Q = I \times \Delta t \quad (2)$$

where C is the calculated capacitance for working electrode, I is the applied current load (A), ΔV is the potential window (0.7 V), Δt is the time of a discharge cycle (s) and m is the mass of cobalt hydroxide (g). Electrochemical impedance spectroscopy (EIS) measurements were also carried out over the frequency range from 10 kHz to 0.1 Hz without DC bias. The EIS data were collected at the open circuit potential, with the AC voltage amplitude of 5 mV.

3. RESULTS AND DISCUSSION

3.1. Physico-chemical characterization

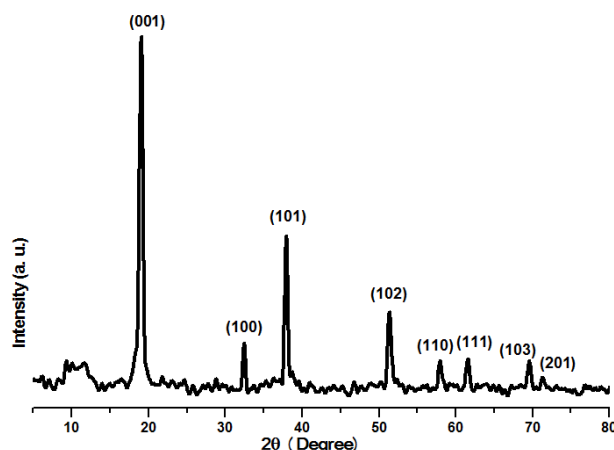


Figure 1. XRD pattern of the hydroxide sample

Fig. 1 shows XRD pattern of the deposited hydroxide through cathodic electrosynthesis. All the observed diffraction patterns are fully matched with the hexagonal brucite-like structure of cobalt hydroxide i.e. $\beta\text{-Co(OH)}_2$ phase, JCPDS file#74-1057. No any diffraction peaks originating from $\alpha\text{-Co(OH)}_2$, indicating that the prepared hydroxide has pure $\beta\text{-Co(OH)}_2$ composition. Furthermore, the

diffraction peak of (001) has high intensity with respect to the other diffraction peaks, showing the preferred orientation/or growth of the cobalt hydroxide with the c-axis [39], as observed by FE-SEM (Figs. 3a and b). The XRD data clearly confirmed that the pure cobalt hydroxide with hexagonal brucite-like structure can be easily prepared through our applied electrochemical procedure.

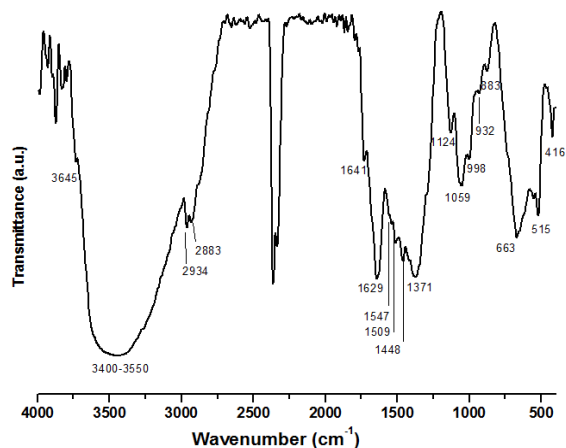


Figure 2. IR spectrum of the hydroxide sample

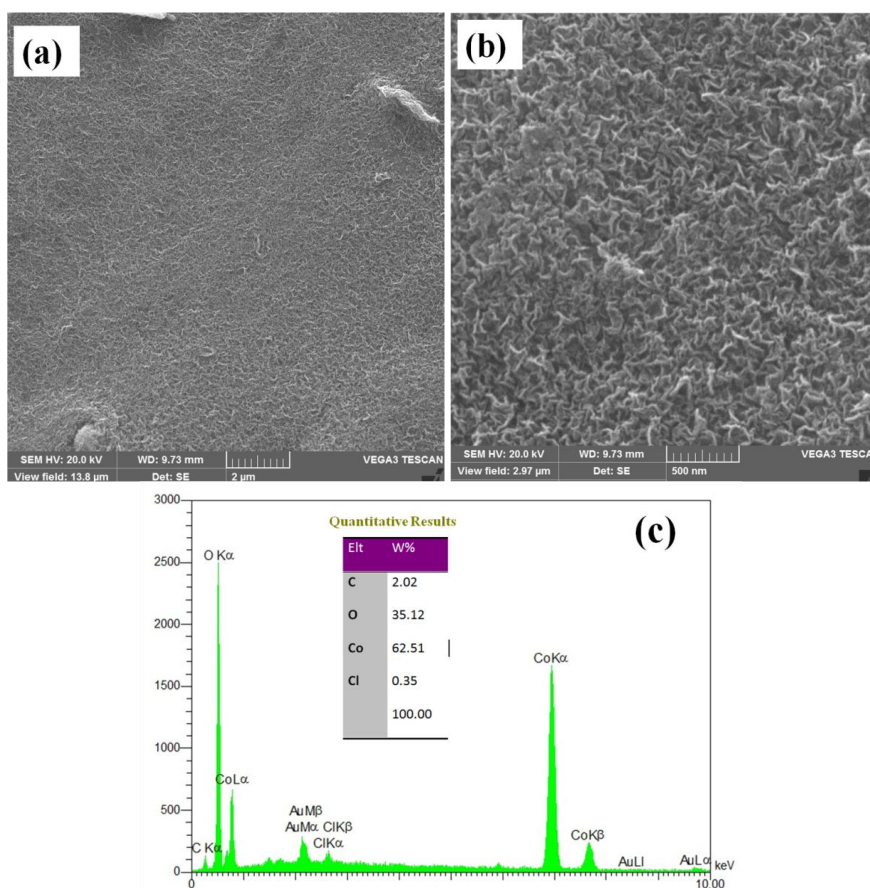


Figure 3. (a,b) FE-SEM images and (c) EDS analysis of the deposited cobalt hydroxide

The IR spectrum of the prepared cobalt hydroxide powder is presented in Fig. 3. From this Figure, it can be clearly observed that the IR spectrum has special absorption peaks corresponding to the β -Co(OH)₂ phase. In this regard, (i) the band at 3645 cm⁻¹ corresponds to the $\nu_{\text{O-H}}$ stretching of the OH groups in the brucite-like structure [12,14], (ii) the two main bands below 700 cm⁻¹ i.e. 663 cm⁻¹, 515 cm⁻¹ and 416 cm⁻¹ are related to the $\delta_{(\text{Co-O-H})}$ and $\gamma_{(\text{Co-O})}$, in the brucite-like octahedron [39-42], (iii) the broad band at 3400-3550 cm⁻¹ is due to the stretch vibrations of hydroxyl groups in the composition of the deposit i.e. OH groups of cobalt hydroxide, adsorbed water molecules and sucrose, (v) the peak at 1641 cm⁻¹ can be assigned to the water molecule vibrations, (vi) the vibrations of various bonds of sucrose is also clearly observable in the IR spectrum (Fig. 2); CH₂ asymmetric and symmetric stretching at 2934 cm⁻¹ and 2878 cm⁻¹, respectively [43], CH₂ scissoring, wagging and twisting at 1448 cm⁻¹, 1371 cm⁻¹ and 1275 cm⁻¹, respectively, C-O-C skeletal mode vibrations at 932 cm⁻¹ [44], C-O stretching of the C-O-H group at 1124 cm⁻¹ and C-O ether bond of the glucose ring at 998 cm⁻¹ [44,45], C-H deformation at 883 cm⁻¹, C-H bending at C-O-H bending at 1059 cm⁻¹ [45]. These IR data clearly confirmed the brucite-like structure (i.e. β -Co(OH)₂ phase) of the deposited hydroxide.

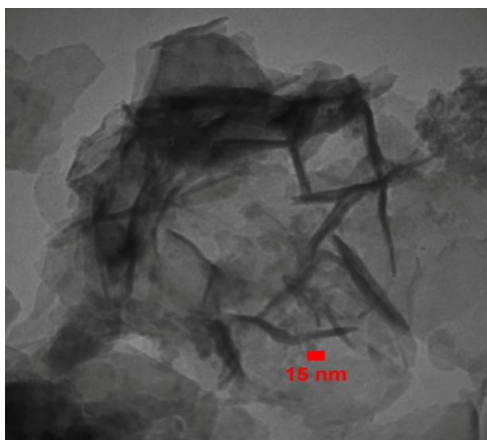


Figure 4. TEM image of the deposited cobalt hydroxide

The surface morphology of the prepared hydroxide was observed through FE-SEM and the images are shown in Fig. 3. From Fig. 3a, it can be seen that the deposited hydroxide has uniform surface morphology at micro scale revealing the uniformity of the deposition conditions i.e. deposit formation and growth during whole time of deposition. From this Figure, it is also seen that the surface of hydroxide has some roughness. High magnification image in Fig. 3b clearly revealed that the deposited hydroxide has lumpy and uneven surface at all area. This form of morphology can provide the sample to have large surface area and pores, which can enable the prepared electroactive material to exhibit better supercapacitive performance. From the observation in Fig. 3b, it is seen that sample morphology has composed of layered thin plates which look like flakes. Also, it seems that the most of flakes had vertical growth direction during deposition process on the cathode surface. High magnification by TEM indicates that the sample has very thin flake-like morphology (Fig. 4). The observed flakes have mostly vertical arrangement or free standing array with sizes about 50 nm.

Notably, some hexagonal forms are seen for the nanoflakes in the TEM images (Fig. 4). Elemental analysis of the prepared cobalt hydroxide is also provided via FE-SEM technique and shown in Fig. 3c. It was found that the deposited sample have the elements of C, O, Cl and Co in its composition. The carbon comes from the sucrose add into the deposition bath, which has been attached on the surface of hydroxide deposited during the electrochemical process. Also, presence of Cl in the composition of the prepared sample is due to the intercalation of chloride ions in the cobalt hydroxide structure. Notably, the chloride/nitrate ions intercalation into the hydroxide structure during cathodic electrodeposition of metal hydroxides from metal nitrate or chloride electrolytes is a confirmed common issue [46-48].

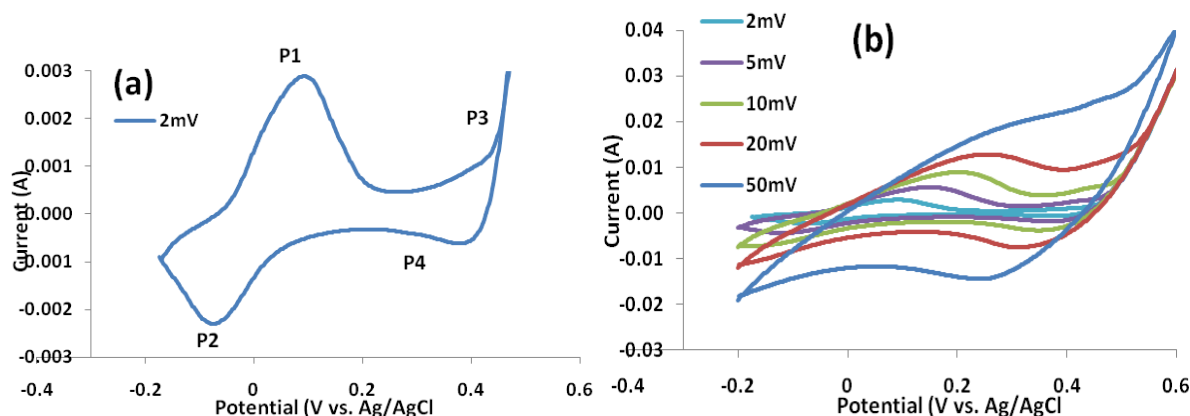
3.2. Electrochemical characterizations

3.2.1. Cyclic voltammetry

Cyclic voltammetry (CV) and galvanostat charge-discharge (GSD) techniques were applied to determine the charge storage ability of the prepared cobalt hydroxide nanoflakes. Fig. 5 presents the cyclic voltammetry curves of the fabricated cobalt hydroxide electrode in 1M KOH at the various scan rates and the exhibited capacitances by the electrode at each applied scan rate. The functional potential range (i.e. -0.2 to 0.6 V vs. Ag/AgCl) for the fabricated electrode was determined through recording one cycle CV between -1V to 1V. For the fabricated electrode, good symmetry of anodic and cathodic peaks from the CV profiles indicates the proper reversibility (Figs. 5a and b). Each curve in CV profiles manifests two pairs of strong redox peaks (i.e. p₁/p₂ and p₃/p₄ as donated in Fig. 5a), which originate from a superior pseudocapacitor nature provided by the following redox reactions [49]:



As can be seen in Fig. 5b, with increasing the scan rates from 5 to 50 mV s⁻¹, the current density increases and the positions of anodic and cathodic peaks shift to the more positive and negative direction, respectively.



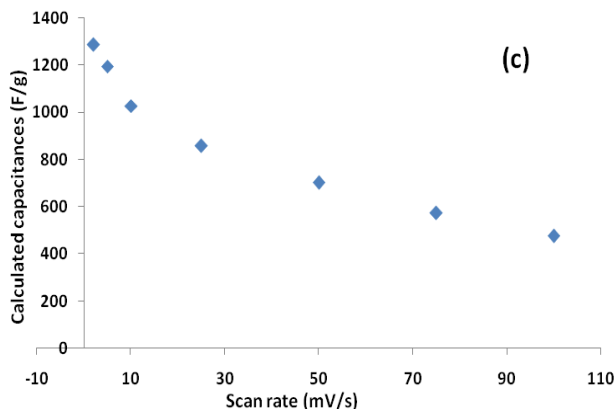
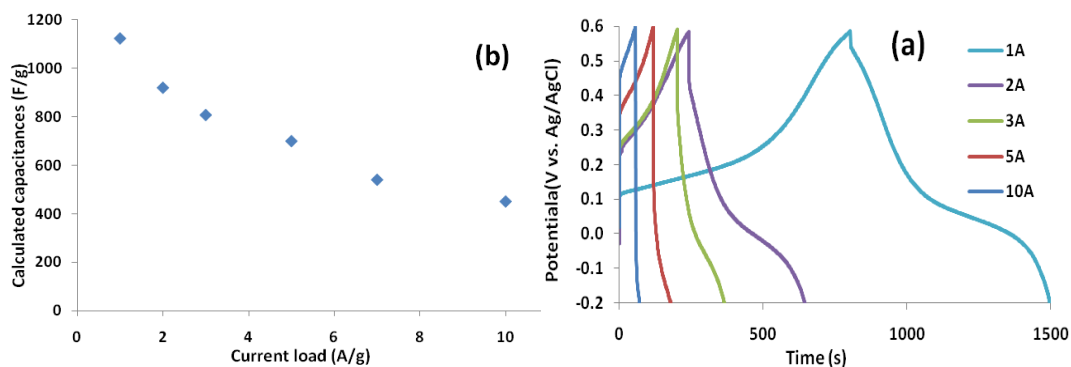


Figure 5. (a) CV profiles of the fabricated cobalt hydroxide electrode at 2 mV/s, and (b) at the various scan rates of 2, 5, 10, 20 and 50 mV/s, and (c) the calculated specific capacitances at the applied scan rates

This change in peak location can be related to the internal resistance of the prepared electrode material [49]. The specific capacitances of the prepared cobalt hydroxide material were calculated from the CV profiles in Fig. 6 through Eq. (1). Fig. 5c shows the calculated SCs at the different applied potential sweeps. It was calculated that the cobalt hydroxide nanoflakes are able to hand over the capacitance values of 1288.1, 1195.6, 1027.3, 878.2, 702.8, 574 and 476.5 F/g at the scan rates of 5, 10, 20, 50, 75 and 100 mV s⁻¹, respectively. The values implicated an excellent supercapacitive performance of the prepared hydroxide nanoflakes.

3.2.2. Charge-discharge tests

Fig. 6a displays the recorded GCD curves of the fabricated electrode at various current loads of 1, 2, 3, 5 and 10 A g⁻¹. Nearly symmetric mode of potential-time curves insinuates the high charge/discharge columbic efficiency and low polarization value for the β-Co(OH)₂ nanoflakes. Notably, a small IR drop is seen on the discharge part of all GCD curves in Fig. 6a. In fact, these instantaneous voltage drops indicating the voltage change due to the ‘current interrupt’ resistance (R_{current interrupt}) [14,50], which become less with decreasing the current density. The SC values were calculated from the GCD curves according to Eq. 2 and plotted in Fig. 6c.



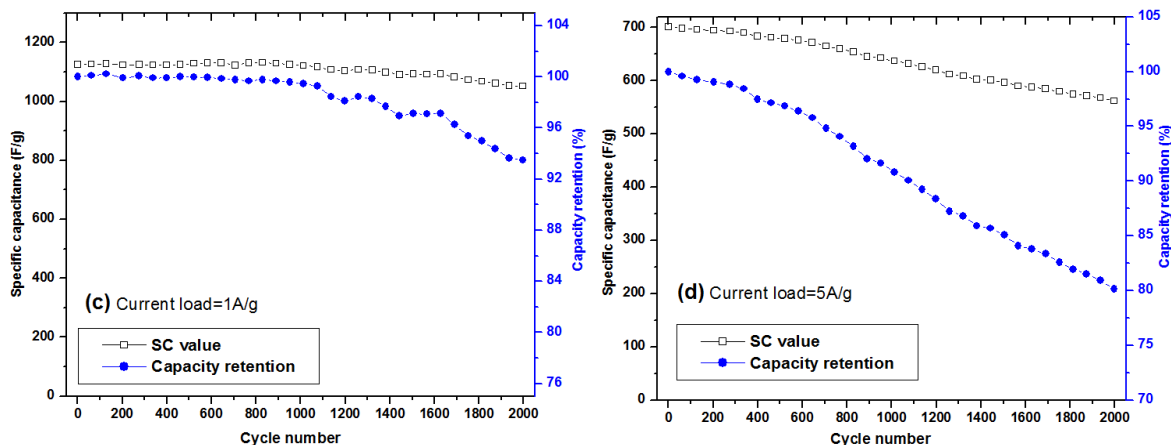


Figure 6. (a) the GCD profiles and (c) calculated SCs at the different current loads, (c,d) specific caapcity values and capacity retention for 2000 GCD cycling at the current load of 1 and 5 A g⁻¹

The calculations indicted that the prepared β -Co(OH)₂ flakes exhibit the capacitances of 1125.4, 992, 849.3, 701.6 and 452.5 F g⁻¹ at 1, 2, 3, 5 and 10 A g⁻¹, respectively (Fig. 6c).

These values show an excellent charge storage ability of the prepared nanoflakes. Moreover, the capacitive performance of our fabricated electrode is comparable with the reported capacitances for the nanostructured cobalt hydroxide in the literature; e.g. 1215.8 F g⁻¹ at the current load of 1 A g⁻¹ for β -Co(OH)₂ nanocapsules [29], 728.5 F g⁻¹ at the discharge current load of 1 A g⁻¹ for β -Co(OH)₂ disc-like nanostructures [32], 1105.3 F g⁻¹ at 1 A g⁻¹ for β -Co(OH)₂ nanoplates [34], 567.1 F g⁻¹ at 1 A g⁻¹ for α -Co(OH)₂ nanosheets [36], 709.1 F g⁻¹ at a current density of 1 A g⁻¹ for cobalt hydroxide nanoplates doped with Al³⁺ ions [38], 1048 F g⁻¹ at a current density of 1 A g⁻¹ for 3D sponge-like Co/Co(OH)₂ nanocomposite [39], 855.4 C g⁻¹ at 1 A g⁻¹ for mixed cobalt/nickel hydroxides [41], 420 F g⁻¹ at 1 A g⁻¹ for Co(OH)₂ nanocubes [42], and 947.3 F g⁻¹ at 1 A g⁻¹ for β -Co(OH)₂ nano-leaves [54].

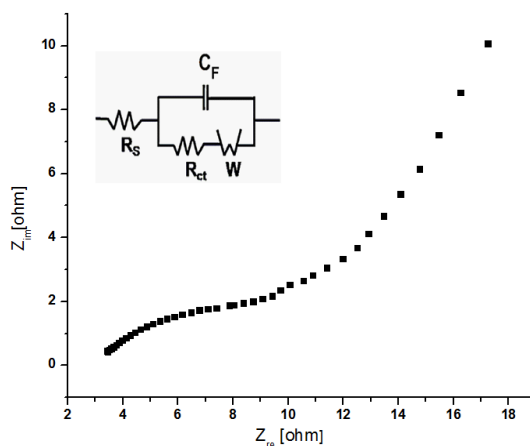


Figure 7. Nyquist plot of the β -Co(OH)₂ electrode with suggested equivalent circuit model

The capacity retention of the prepared nanomaterials was also evaluated through 2000 GCD cycling at the current loads of 1 and 5 A g⁻¹. The observed results i.e. specific capacitances and capacity retentions are shown in Fig. 6c. It was observed that the charge storage of the prepared nanoflakes are reduced from 1125.4 F g⁻¹ to 1052.1 F g⁻¹ after 2000 cycling at 1 A g⁻¹, which indicates the 93.48% capacity retention. Also, our electrode capacity is dropped from 701.6 F g⁻¹ to 562.4 F g⁻¹ after 2000 GCD at current load of 5 A g⁻¹ showing the 80.17% capacity retention. These results confirmed that the prepared cobalt hydroxide nanoflakes have proper cycle life.

3.2.3. EIS measurements

Fig.7 demonstrates the EIS plot of the β -Co(OH)₂-based electrode under open circuit potential in the frequency range of 10Hz to 100 kHz. This plot exhibits a semicircular followed by nearly straight line. It can be fitted to the behavior of an equivalent circuit comprising an equivalent series resistance (R_s), double layer capacitor (C_{dl}), a charge transfer resistance (R_{ct}), a Warburg element (Z_w) and a pseudocapacitance (C_p) (as shown in inset of Fig. 7. The R_s and R_{ct} are the limiting factors of any electrode material [43-45]. R_s can be acquired from the x intercept of the EIS plot. R_{ct} is equivalent to the diameter of the semicircular on EIS plot. In the case of the β -Co(OH)₂based electrode, the R_s and R_{ct} were 3.25 Ω and 1.32 Ω , respectively. These relative low R_s and R_{ct} values implicates that the electrode could exhibit suitable capacitive performance. Also, the nearly ideal straight line observed at lower frequencies which is indicative of the low diffusion resistance of β -Co(OH)₂ nanoflakes. All of these results are in line with confirming the good electrochemical capacitive properties of our prepared material.

4. CONCLUSION

The constant current cathodic electrodeposition of cobalt hydroxide was performed from aqueous cobalt chloride with saccharide additive. The XRD and IR analyses revealed that the prepared deposit has brucite-type cobalt hydroxide crystal structure. The SEM and TEM observations showed flake-like nanostructures for the deposited sample. The specific capacitances of 1288.1, 1195.6, 1027.3, 878.2, 702.8, 574 and 476.5 were measured through cyclic voltammetry at the scan rates of 5, 10, 20, 50, 75 and 100 mV s⁻¹, respectively. These findings proved that our electro-synthesized nanomaterials have proper charge storage ability and can be used in supercapacitors.

ACKNOWLEDGEMENTS

The authors thank the research council of University of Tehran for financial support of this work.

References

1. Y. Wang, Y. Song, and Y. Xia, *Chem. Soc. Rev.*, 45 (2016) 5925.

2. M. Aghazadeh, A. Nozad Golikand, and M. Ghaemi, *Int. J. Hydrogen Energy*, 36 (2011) 8674.
3. J. S. Shayeh, A. Ehsani, M. R. Ganjali, P. Norouzi, and B. Jaleh, *Applied Surface Science* 353 (2015) 594.
4. K. Adib, M. Rahimi-Nasrabadi, Z. Rezvani, S.M. Pourmortazavi, F Ahmadi, H. R. Naderi, and M. R. Ganjali, *J. Mater. Sci.* 27 (2016) 4541.
5. H. Gholipour-Ranjbar, M. R. Ganjali, P. Norouzi and H.R. Naderi, *J. Mater. Sci. Mater. Electron.*, 27 (2016) 10163.
6. H. R. Naderi, P. Norouzi and M. R. Ganjali, *Appl. Surf. Sci.*, 366 (2016) 552.
7. H. Gholipour-Ranjbar, M. R. Ganjali, P. Norouzi and H.R. Naderi, *J. Mater. Sci. Mater. Electron.*, 27 (2016) 10163.
8. H. Gholipour-Ranjbar, M.R. Ganjali, P. Norouzi, and H.R. Naderi, *Ceram. Int.*, 42 (2016) 12097.
9. H. R. Naderi, M. R. Ganjali, and P. Norouzi, *Int. J. Electrochem. Sci.*, 11 (2016) 4267.
10. H.R. Naderi, M.R. Ganjali, A.S. Dezfouli, and P. Norouzi, *RSC Adv.*, 6 (2016) 51211.
11. M. Aghazadeh, A.A.M. Barmi, D. Gharailou, M.H. Peyrovi, and B. Sabour, *Appl. Surf. Sci.*, 283 (2013) 871.
12. A. Barani, M. Aghazadeh, M.R. Ganjali, B. Sabour, A.A.M. Barmi, and S. Dalvand, *Mater. Sci. Semiconduct. Process.*, 23 (2014) 85.
13. T. Yousefi, A. Nozad Golikand, M.H. Mashhadizadeh, and M. Aghazadeh, *Curr. Appl. Phys.*, 12 (2012) 193.
14. A.A.M. Barmi, M. Aghazadeh, B. Arhami, H.M. Shiri, A.A. Fazl, and E. Jangju, *Chem. Phys. Lett.*, 541 (2012) 65.
15. X. Wang, C. Chen, K. Chen, H. Chen, and S.J. Yuan, *Int. J. Electrochem. Sci.*, 11 (2016) 3425.
16. M. Aghazadeh, A. Rashidi, and M.R. Ganjali, *Int. J. Electrochem. Sci.*, 11 (2016) 11002.
17. M. Aghazadeh, A. Bahrami-Samani, D. Gharailou, M.G. Maragheh, and M.R. Ganjali, *J. Mater. Sci.: Mater. Electron.*, 27 (2016) 11192.
18. M. Aghazadeh, R. Ahmadi, D. Gharailou, M.R. Ganjali, and P Norouzi, *J. Mater. Sci.: Mater. Electron.*, 27 (2016) 8623.
19. P. Razmjoo, B. Sabour, S. Dalvand, M. Aghazadeh, and M.R. Ganjali, *J. Electrochem. Soci.*, 161 (2014), D293.
20. M. Aghazadeh, M.G. Maragheh, M.R. Ganjali, and P Norouzi, *RSC Adv.*, 6 (2016) 10442.
21. T. Yousefi, A. NozadGolikand, M.H. Mashhadizadeh, and M. Aghazadeh, *Curr. Appl. Phys.*, 12 (2012) 544.
22. M. Aghazadeh, M.R. Ganjali, and P. Norouzi, *J. Mater. Sci.: Mater. Electron.*, 27 (2016) 7707.
23. M. Aghazadeh, B. Sabour, M.R. Ganjali, and S. Dalvand, *Appl. Surf. Sci.*, 313 (2014) 581.
24. M. Aghazadeh, M.G. Maragheh, M.R. Ganjali, P. Norouzi, and F. Faridbod, *Appl. Surf. Sci.*, 364 (2016) 141.
25. K. Sun, H. Wang, H. Peng, Y. Wu, G. Ma, and Z. Lei, *Int. J. Electrochem. Sci.*, 10 (2015) 2000.
26. M. Aghazadeh, M. Asadi, M.G. Maragheh, M.R. Ganjali, and P. Norouzi, *Appl. Surf. Sci.*, 364 (2016) 726.
27. H. Gholipour-Ranjbar, M.R. Ganjali, P. Norouzi, and H.R. Naderi, *Mater. Res. Express*, 3 (2016) 075501
28. H.R. Naderi, P. Norouzi, M.R. Ganjali, and H. Gholipour-Ranjbar, *Powder Technol.*, 302 (2016) 298.
29. M. Aghazadeh, and S. Dalvand, *J. Electrochem. Soc.*, 161 (2014) D18.
30. M. Aghazadeh, M. Hosseini-fard, B. Sabour, and S. Dalvand, *Appl. Surf. Sci.*, 287 (2013) 187.
31. J. Tizfahm, M. Aghazadeh, M. G. Maragheh, M. R. Ganjali, P. Norouzi, *Mater. Lett.*, 167 (2016) 153.
32. M. Aghazadeh, H.M. Shiri, and A.A.M. Barmi, *Appl. Surf. Sci.*, 273 (2013), 237.
33. J. Talat Mehrabad, M. Aghazadeh, M. Ghannadi Maragheh, and M.R. Ganjali, *Mater. Lett.*, 184 (2016) 223.

34. M. Aghazadeh, S. Dalvand, and M. Hosseinifard, *Ceram. Int.*, 40 (2014) 3485.
35. J. Hyeon Lee, Y. Du, and D. O'Hare, *Chem. Mater.*, 21 (2009) 963.
36. J.P. Cheng, L. Liu, K.Y. Ma, X. Wang, Q.Q. Li, J.S. Wu, and F. Liu, *J. Colloid Interface Sci.*, 486 (2017) 344.
37. T. Nguyen, M. Boudard, M.J. Carmezim, M.F. Montemor, *Energy*, 126 (2017) 208.
38. R. Liu, Z. Jiang, J. Ma, L. Ni, X. Sun, Y. Liu, H. Chen, and Q. Liu, *RSC Adv.*, 7 (2017) 3783.
39. T. Xu, L. Zhao, Z. Wu, Y. Liu, Z. Zeng, K. Zhu, and G. Li, *Mater. Lett.*, 186 (2017) 74.
40. Y. Zhang, J. Wu, T.X. Zheng, Y.X. Zhang, and H. Liu, *Mater. Technol.*, 31 (2016) 521.
41. X.i Meng, M. Feng, H. Zhang, Z. Ma, and C. Zhang, *J. Alloys Compd.*, 695 (2017) 3522.
42. J. Yang, X. Zhang, Z. Xu, J. Huang, J. Chen, *J. Electroanal. Chem.*, 788 (2017) 54.
43. I. Karimzadeh, M. Aghazadeh, M.R. Ganjali, P. Norouzi, and T. Doroudi, *Mater. Lett.*, 189 (2017) 290.
44. M. H. Khanmirzaei, and S. Ramesh, *Int. J. Electrochem. Sci.*, 8 (2013) 9977.
45. I. Karimzadeh, M. Aghazadeh, M.R. Ganjali, P. Norouzi, and S. Shirvani-Arani, *Mater. Lett.*, 179 (2016) 5.
46. M. Aghazadeh, A.A.M. Barmi, H.M. Shiri, and S. Sedaghat, *Ceram. Int.*, 39 (2013) 1045.
47. M. Aghazadeh, B. Arhami, A.-A. Malek Barmi, M. Hosseinifard, D. Gharailou, and F. Fathollahi, *Mater. Lett.*, 115 (2014) 68.
48. F. Abed, M. Aghazadeh, and B. Arhami, *Mater. Lett.*, 99 (2013) 11.
49. Rusi, and S.R. Majid, *Scientific Reports*, 5 (2015) 16195.
50. C. Yuan, L. Hou, L. Shen, D. Li, F. Zhang, C. Fan, J. Li, X. Zhang, *Electrochim. Acta*, 56 (2010) 115.
51. H. Ma, J. He, D.-B. Xiong, J. Wu, Q. Li, V. Dravid, and Y. Zhao, *ACS Appl. Mater. Interfaces*, 8 (2016) 1992.
52. G. Yu, L. Hu, M. Vosgueritchian, H. Wang, X. Xie, J. R. McDonough, X. Cui, Y. Cui, and Z. Bao, *Nano Lett.*, 11 (2011) 2905.
53. C. Ogata, R. Kurogi, K. Hatakeyama, T. Taniguchi, M. Koinuma, and Y. Matsumoto, *Chem. Commun.*, 52 (2016) 3919.
54. M. Aghazadeh, A.A. Malek Barmi, and T. Yousefi, *J. Iranian Chem. Soc.*, 9 (2012) 225.

© 2017 The Authors. Published by ESG (www.electrochemsci.org). This article is an open access article distributed under the terms and conditions of the Creative Commons Attribution license (<http://creativecommons.org/licenses/by/4.0/>).